AIP | Biomicrofluidics

Sample preconcentration inside sessile droplets using electrowetting

Dileep Mampallil, Dhirendra Tiwari, Dirk van den Ende, and Frieder Mugele

Citation: Biomicrofluidics **7**, 044102 (2013); doi: 10.1063/1.4815931
View online: http://dx.doi.org/10.1063/1.4815931
View Table of Contents: http://bmf.aip.org/resource/1/BIOMGB/v7/i4
Published by the AIP Publishing LLC.

Sample preconcentration inside sessile droplets using electrowetting

Dileep Mampallil, Dhirendra Tiwari, Dirk van den Ende, and Frieder Mugele[a)]
Physics of Complex Fluids, MESA + Institute, Department of Science and Technology, University of Twente, P.O. Box 217, 7500 AE Enschede, The Netherlands

(Received 20 May 2013; accepted 2 July 2013; published online 12 July 2013)

Electrowetting with alternate voltage (AC) creates azimuthal flow vortices inside sessile droplets. These flow vortices can be controlled by introducing pinning sites at the contact line. When the frequency of the applied AC voltage is gradually ramped from a few hundreds of hertz to a few tens of kilohertz the azimuthal flow vortices contract and move towards the contact line near the pinning site. Dispersed particles in the liquid are collected in the center of these vortices leading to an increase in the local particle concentration by up to more than one order of magnitude. We provide a qualitative explanation for symmetry of the flow patterns within the drops and discuss possible scenarios explaining the particle collection and preconcentration. © *2013 AIP Publishing LLC*.
[http://dx.doi.org/10.1063/1.4815931]

I. INTRODUCTION

Microfluidic techniques have the advantage of consuming only a little amount of sample for biochemical analyses. When the sample contains analyte at very low concentration, it is essential to improve the sensitivity of such techniques. Improving the sensitivity of the detection system can be complicated and expensive. Alternatively, a sample preconcentration can be performed within the lab on chip devices. Examples reported in the literature include microfluidic trapping and concentration of mRNA,[1] on chip preconcentration through hydrodynamic filtering,[2] bubble microstreaming,[3] surface acoustic waves,[4] or methods based on surface binding, porous membranes, nano channels, solvent extraction, or velocity gradients as reviewed by Lin *et al.*[5] Most of the above mentioned techniques are applied in continuous flow microfluidics.

Sample preconcentration can also be beneficial in droplet based microfluidics. Particles or cells in droplets (also in continuous flow) can be ordered deterministically using Dean flow[6–8] for further separation from the liquid phase. Particles in the droplets can also be concentrated by magnetic[9,10] or electrophoretic[11] forces and can be separated by splitting the droplet using electrowetting.[12] Karimi *et al.*[13] recently discussed various hydrodynamic mechanisms of cell and particle trapping, including, in particular, low Reynolds number steady streaming. He *et al.* demonstrated that solutes and particles entrapped in aqueous micro droplets in ambient oil phase can be concentrated by letting the water molecules from the droplet dissolve into the organic phase.[14] In a similar manner, Abdelgawad *et al.* demonstrated enrichment of oligonucleotides from a solution containing histones by driving the droplet into water-immiscible phenolic solution for liquid extraction.[15] Another method is to extract solid phase from liquid by driving the droplets over a porous polymer monolith disc.[16] Evaporation of solvent is another approach analogue to solvent extraction and has recently also been adapted to drops in microfluidic channels.[17]

Methods that require solvent extraction or evaporation or specific pH values or solvent conductivity of the fluid for optimal performance are not always compatible with biological applications. Fluid mechanical methods that generate concentration gradients in a passive

[a)]Author to whom correspondence should be addressed. Electronic mail: f.mugele@tnw.utwente.nl

manner due to interactions of solutes with the flow field and/or amongst each other provide an interesting alternative. The fundamental interactions are rather complex and involve inertial forces such as centrifugal forces and lift forces, as well as viscous forces in shear flows with and without gradients and hydrodynamic forces between solute particles.[7,18–23] Secondary flows such as Dean flows generated by fluid motion in curved paths have recently attracted increasing attention. These mechanisms are completely non-invasive regarding the composition of the fluid and the presence of external fields. In electrowetting (EW)-based microfluidics, internal flows within drops can be generated by moving drops back and forth within the typical sandwich geometry of Lab-on-a-Chip devices[24,25] or exciting sessile drops on a planar surface with alternate voltage (AC) over a wide frequency range. Depending on the applied frequency, the driving mechanism to excite the flows can be either hydrodynamic (at low frequencies)[26–30] or electrothermal[28,31] if the electric fields penetrate into the liquid. From an applied perspective, the previous studies focused on promoting mixing. In the hydrodynamic low frequency regime, it was shown that capillary waves traveling from the contact line towards the apex of the drop are responsible for driving the internal flow[29,32] following the so-called Stokes drift mechanism. Understanding the physical origin of the internal flow fields enables novel applications, such as the suppression of the coffee stain effect in evaporating drops of complex fluids,[33] which results—amongst others—in improved sample preparation protocol for MALDI mass spectrometry.[34] Recently, we also demonstrated that the symmetry of the internal flow fields can be controlled by blocking the motion of the contact line locally at pinning sites added to the surface.[35]

In this article, we show that by controlling the flow patterns, we can achieve the inverse of mixing, namely sample preconcentration within sessile droplets. We enhance the local concentration of colloidal particles in a sessile droplet using AC electrowetting. This is accomplished by sweeping the frequency of the applied voltage from a low (∼1 kHz) to a high (∼40 kHz) value, while part of the contact line is immobilized using artificial pinning sites. A single pinning site creates two well defined azimuthal (plane parallel to the substrate) flow vortices inside the droplet in the plane of the solid surface.[35] By gradually increasing the frequency, these flow vortices can be shifted towards the pinning site. The particles are trapped at the center of the vortices and finally collected near the pinning site. We provide an explanation of the azimuthal flow fields within the drops and discuss the possible mechanisms of the particle collection.

II. EXPERIMENTS

The experimental setup is illustrated in Figs. 1(a) and 1(b). It contains an indium tin oxide (ITO) coated glass covered with SU8 dielectric layer. SU8 layers are moderately hydrophobic with Young's contact angle about 85°. Lithographically coated gold stripes (size: O(500 μm)) or even simple patches of silver paste act as the electrodes on the SU8 layer. Droplets of volume ranging between 0.4 and 1 μl are deposited on the SU8 layer such that the contact line partially pins on the electrode. In all the measurements, droplets contained 10 mM KCl salt solution prepared in deionized water. The droplets also contained fluorescently labelled polystyrene colloidal particles of diameter ranging from 0.02 to 7.8 μm with volume fraction of 0.05%.

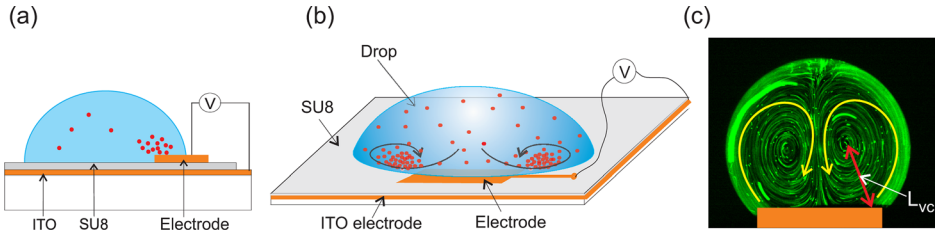

FIG. 1. The side view (a) and the top view (b) of the experimental setup. In a bottom view image (c) of a real droplet, the direction of the flow vortices is shown. The distance between the vortex center and the pinning site L_{vc} is represented by the red arrow. The orange rectangle represents the electrode where the contact line of the droplet is pinned.

A voltage of 150 V (resulting in a contact angle of about 50°) is applied between the ITO layer and the electrode. The frequency of the applied voltage, f_{AC} is swept from 1 kHz to typically 40 kHz with a typical rate of 1 kHz/s. Note that the EW force is proportional to the square of the applied voltage.[12] Therefore, the hydrodynamic driving frequency experienced by the drop is 2 f_{AC}. A confocal microscope is used to observe the particles in a plane typically about 100 μm above the transparent substrate. An exposure time of 0.5 s is used to image the colloidal particles. Typical flow velocity involved in the droplet is about 1 mm/s (also see Ref. 35). Dedicated experiments to characterize the azimuthal flow velocity in the vortex were carried out using a high speed camera (Photron SA3) at a frame rate of 125 frames/s, while sweeping the frequency from 1 to 20 kHz at a rate of 1 kHz/s. The azimuthal flow velocities at different radial distances from the vortex center were obtained by tracking[36] the tracer particles.

III. RESULTS

When the voltage is applied flow vortices appear as shown in Fig. 1(c). In Fig. 2(a), we show typical bottom view images of droplets in the initial and final stages of the preconcentration process. The droplets contain 0.02 μm, 0.5 μm, and 5 μm particles. The top row shows the droplets in the beginning of the frequency sweep ($t = 0$ and $f_{AC} = 1$ kHz) and the bottom row shows those at the end ($t = t_{fin}$ and $f_{AC} = 40$ kHz). For 5 μm particles, two large flow vortices are visible at 1 kHz frequency. For the other droplets, the vortices are not visible due to the small size of the particles. Upon increasing the frequency, the flow vortices get smaller and shift towards the pinning region while collecting the particles along with them. Each flow vortex thus concentrates particles separately near the edge of the pinning site (see the movie in Fig. 2). Therefore, the fluorescent intensity at two places near the pinning site is increased as seen from Fig. 2. In our experiments, we observed intensity enhancements (=*final maximum intensity*/*initial average intensity*) by a factor of 11 ± 2, 9 ± 2, and 6 ± 4 for the droplets with particles of diameter 5 μm, 0.5 μm, and 0.02 μm, respectively.

Applying a fixed low frequency, for example, 1 kHz without sweeping, no noticeable particle accumulation in the center of the vortices is observed. However, when a fixed high frequency say, 40 kHz is applied for 30 s the small vortices formed near the pinning sites collect a few number of particles (diameter of 5 μm) producing an intensity enhancement by about a factor 4. We observed that a slow frequency sweep is important because it helps collecting extra particles at the vortex center in time. As the frequency increases, the intensity at the

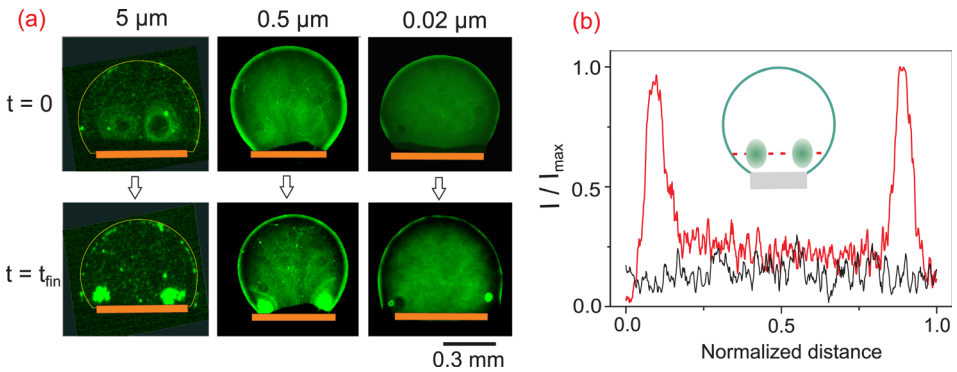

FIG. 2. (a) The bottom view images of the droplets with colloidal polystyrene particles of diameter 5 μm, 0.5 μm, and 0.02 μm. The top and the bottom rows represent droplets in the beginning ($t = 0$ and $f_{AC} = 1$ kHz) and at the end ($t = t_{fin}$ and $f_{AC} = 40$ kHz) of the frequency sweep, respectively. The bright rim of the droplets is due to reflection. The orange rectangles represent the position of the pinning site, i.e., the electrode (enhanced online) [URL: http://dx.doi.org/10.1063/1.4815931.1]. (b) The intensity profile for the droplet containing 0.5 μm particles before (black) and after (red) the frequency sweep. The intensity is normalized with respect to its maximum value. Distance is normalized with respect to the total profiling length. The inset is a cartoon of the droplet with the dashed line indicating the location of the intensity profile.

vortex centers increases with time due to the accumulation of the fluorescent particles as plotted in Fig. 3. The larger particles are accumulated faster and more efficiently than the smaller ones.

The existence of the flow vortices is obviously crucial for the preconcentration process. There is a clear correlation between the efficiency of the preconcentration and the dynamics of the vortices. Therefore, we studied their behavior as a function of the applied frequency for a variety of drop sizes. In Fig. 4, we show the position of the vortex core L_{vc} as a function of the applied frequency. We take the distance between the pinning site and the vortex-center as a characteristic measure of the position of a vortex (see Fig. 1(c) and also Ref. 35)). While the overall size of the vortex and position of its core decreases with increasing f_{AC}, the exact values of the initial and final value of the ramp frequency seem to have little influence on the preconcentration process. The initial value should be about a few hundred hertz, in a range above the lowest eigenfrequencies of the drop. Below about 200 Hz, we do not observe substantial flows in the azimuthal direction (see also Ref. 35). Particle collection only becomes efficient beyond an onset frequency (marked by the arrows in Fig. 4) where the vortex cores begin to shift. The onset frequency increases with decreasing drop size. From a practical perspective, the initial value of the frequency sweep is best chosen just below the onset frequency. Beyond approximately 20 kHz, the vortices typically hardly move any more. This is also the ideal choice for the maximum sweep frequency.

IV. DISCUSSION

There are two major aspects to understand in order to explain our experiments. First, the origin of the flow vortices and their shifting towards the pinning site and second, the mechanism that collects the particles at the vortex-center.

We note at the outset that despite the maximum frequency of 40 kHz, all experiments remain well within the hydrodynamical regime of EW-driven flows. For the present salt concentration, the onset frequency for electrothermal flows is of order 1 MHz.[28,31] Moreover, test experiments with salt concentrations of 200 mM did not affect the preconcentration process. The azimuthal flow vortices were described experimentally in Ref. 35, yet, we could not explain their origin at that time. In view of the more detailed numerical studies performed recently,[32] such an explanation can now be given: the hydrodynamic flow patterns inside the sessile drops are driven by capillary waves traveling from the contact line upward along the

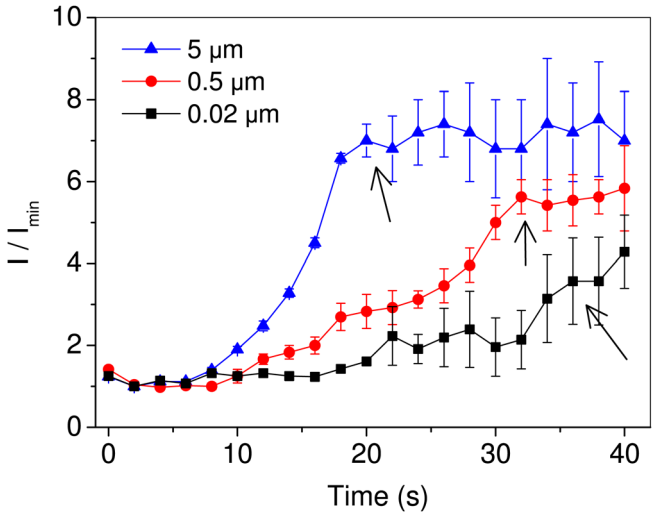

FIG. 3. The intensity at the vortex-center as a function of time for a frequency sweep from 1 to 40 kHz at a rate of 1 kHz/s. The amount of particles accumulated reaches a maximum and does not increase any further. Larger particles reach this maximum amount quicker (marked by the arrows) than the smaller ones. The normalization is performed with respect to the average initial intensity for each type of particles. The error bar is the standard deviation in the intensity values for the four vortices in two different droplets of volume 0.7 μl each.

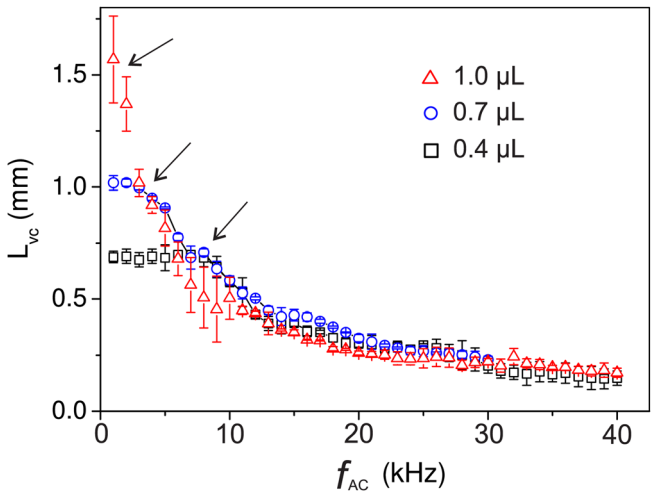

FIG. 4. The displacement of the vortex-center L_{vc} versus frequency for droplets of different volume (shown in the figure). The arrows indicate the onset frequency above which the vortices start to shift. Below this onset frequency, the size of the vortex is comparable to the radius of the droplet. Smaller the droplet the larger the onset frequency. The error bar is the standard deviation in the values of L_{vc} for the four vortices in two different droplets, for each droplet volume.

drop surface following the Stokes drift mechanism. For a cylindrically symmetric drop, material conservation then enforces a downward flow from a stagnation point at the apex of the drop towards the substrate along the symmetry axis as described earlier. This situation can also be observed in the x-z-plane in Fig. 5(a) and results in a similar vortex in the normal plane as in Refs. 29 and 32. In Fig. 5(b), however, the capillary waves are blocked on one side of the drop due to the pinning site. As a consequence, a net flow from the opposite side towards the

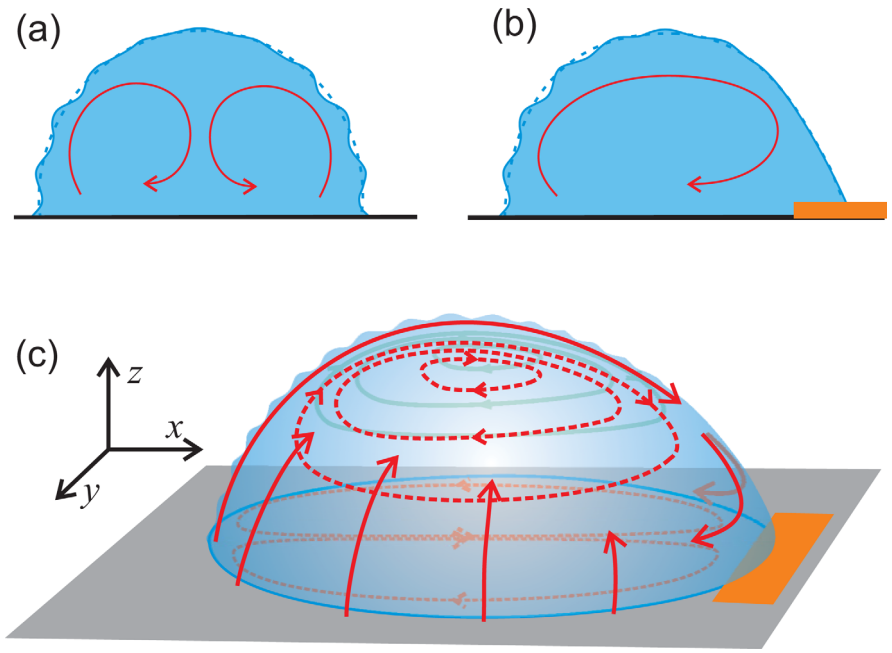

FIG. 5. Cartoon of an AC electrowetting droplet (electric connections are not shown). (a) and (b) are side view and (c) is 3D view. (a) Capillary waves on the surface of the droplet create internal flows (marked by the red, curved arrows) by a Stokes drift like mechanism (see Refs. 29 and 32). (b) When the symmetry is broken by a pinning site, there are no waves and hence no upward flows in the regions near the pinning site. All the upward flows as illustrated by red arrows in (c) sink in the pinning region. Due to mass conservation fluid flows back, creating vortices illustrated by the red dashed lines.

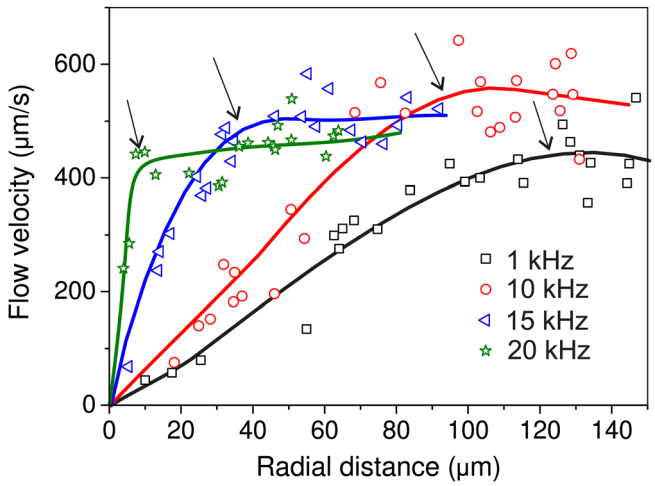

FIG. 6. Azimuthal flow velocity in the vortices at the liquid-air interface as a function of the radial distance from the center of the vortex. The velocity is zero at the center and increases to a large value near the outer boundary (represented by the arrows) of the vortex. As the frequency f_{AC} (shown in the figure) increases, the radius of the vortex decreases and the shear rates increase sharply at the edge of the vortex. The solid lines are guide to the eyes.

pinning site arises, which is superimposed onto the original vortex in the symmetric flow. The stagnation point moves towards the pinning. Seen from below through the substrate this leads to a projected vortex flow that is oriented towards the center of the pinning side and away from its edges, in accordance with the experimental observations.

The contraction of the vortices with increasing frequency follows the scenario described earlier (see Ref. 35). Capillary waves of higher frequency display a shorter wavelength and experience a stronger damping. On a global scale, high frequency capillary waves (i.e., $>$ kHz) are much less efficient in driving the flow.[32] Locally, however, they still act along the three-phase contact line. The contrast between mobile regions of the contact line, where capillary waves generate an upward flow and pinned regions, still leads to local gradients at the edges of the pinning side and is—as the experiments show—still able to drive strong local vortex flows. Obviously, it would be desirable to confirm this scenario by numerical simulations. This would, however, involve very costly three-dimensional simulations, which are beyond the scope of the present communication.

The next step is to understand the physics of particle accumulation process at the center of the vortices. The absence of electric field penetration excludes electrophoretic effects or electro-thermal flows as a possible driving force for the actuation of the solute particles. Therefore, we assume that the particle accumulation is a purely hydrodynamic process.

Shelby *et al.*[37] reported that high radial accelerations can exist in laminar microvortices where particles lighter than the liquid are trapped in the core while the heavier ones are spun away to the outer edge of the vortices. To test the influence of the density mismatch in our system, we performed the following control experiments: in the first case, we used particles lighter than the liquid, i.e., 7.8 μm polystyrene particles (density $= 1.05$ g/cm^3) in heavy water (density $= 1.1$ g/cm^3) and in the second case, particles heavier than the liquid, i.e., 3 μm silica particles (density $= 1.8$ g/cm^3) in water (density $= 1.0$ g/cm^3). In the case of the lighter particles, the accumulation appeared to be at the liquid-air interface, whereas the heavier silica particles settled quickly onto the substrate. Yet, in both cases, preconcentration of particles in the core of the vortices was found demonstrating that simple centrifugal effects are not the governing factor for the particle migration.

Having excluded centrifugal forces, we consider the possibility of particle migration across streamlines due to inertial lift forces.[7,18–23] For example, in annular vortex created in tubular[38] or microchannel,[39] sudden expansion particle migration from continuous segments of the flow to vortices due to lift forces has been reported. Other than simple shear flow, if there are shear gradients (curvature in the velocity profile) additional lift forces can act on the particles. The

data shown in Fig. 6 illustrate that shear and shear gradients are indeed present in our system. Yet, as before, inertial lift forces can be excluded as a source since particle Reynolds number ($R_p = \rho\dot{\gamma}a^2/\eta$, where ρ is the density of the liquid, $\dot{\gamma}$ is the shear rate, a is the particle diameter, and η is the viscosity) should be of order 1 or higher to create noticeable effects.[23] Even for the largest particles in our experiments with $a = 7.8\,\mu$m, R_p is only of order 10^{-3}. We therefore suspect—without proof—that a viscous mechanism similar to the trapping of particles and cells in steady streaming microeddies[40] is responsible for our observations. Even for this well-documented phenomenon, the detailed theoretical understanding only begins to emerge.[41] Clearly, more a systematic theoretical investigation beyond the scope of the present article is needed to elucidate the origin of this complex phenomenon.

We anticipate that our preconcentration technique will be particularly attractive for positioning and concentrating analyte (for example, particles, cells) in drops to improve isolation, collection, and detection. The technique can be integrated in droplet based microfluidics preferably in applications involving sessile drops in configurations such as the "all-terrain droplet actuation" described in Ref. 15. Additional tools of interest include a suitable way of drop splitting to harvest the increased local concentration in a smaller daughter drop as well as a localized detection technique, such as an electrochemical detection that was recently demonstrated in combination with electrowetting.[42] Various combinations with different electrode geometries are conceivable to facilitate ease of handling, parallel processing of many drops, automated drop deposition by inkjet printing.

V. CONCLUSION

In conclusion, we have demonstrated that using AC electrowetting well defined flow vortices can be created in a sessile droplet with locally pinned contact lines. Upon sweeping the applied AC frequency, dispersed particles can be trapped in these vortices and accumulated near edges of the pinning site. Particle accumulation is more efficient for larger particles. The technique can be used as a sample preconcentration method for sessile droplets. Further investigations are to be performed to fine tune the method for various biomolecules and cells inside sessile droplets.

ACKNOWLEDGMENTS

We thank D. Wijnperle for the preparation of the substrates. We acknowledge MicroNed, the Microtechnology Research Programme of The Netherlands, for financial support of project II-B-2 and by NWO, the Dutch science foundation within the NWO-ECHO program.

[1]B. C. Satterfield, S. Stern, M. R. Caplan, K. W. Hukari, and J. A. A. West, Anal. Chem. **79**, 6230 (2007).
[2]M. Yamada and M. Seki, Lab Chip **5**, 1233 (2005).
[3]C. Wang, S. V. Jalikop, and S. Hilgenfeldt, Biomicrofluidics **6**, 012801 (2012).
[4]R. V. Raghavan, J. R. Friend, and L. Y. Yeo, Microfluid. Nanofluid. **8**, 73 (2010).
[5]C.-C. Lin, J.-L. Hsu, and G.-B. Lee, Microfluid. Nanofluid. **10**, 481 (2011).
[6]S. S. Kuntaegowdanahalli, A. A. S. Bhagat, G. Kumar, and I. Papautsky, Lab Chip **9**, 2973 (2009).
[7]D. D. Carlo, Lab Chip **9**, 3038 (2009).
[8]E. W. M. Kemna, R. M. Schoeman, F. Wolbers, I. Vermes, D. A. Weitz, and A. van den Berg, Lab Chip **12**, 2881 (2012).
[9]Y. Wang, Y. Zhao, and S. K. Cho, J. Micromech. Microeng. **17**, 2148 (2007).
[10]A. H. C. Ng, K. Choi, R. P. Luoma, J. M. Robinson, and A. R. Wheeler, Anal. Chem. **84**, 8805 (2012).
[11]S. K. Cho, Y. Zhao, and C.-J. Kim, Lab Chip **7**, 490 (2007).
[12]F. Mugele and J. C. Baret, J. Phys. Condens. Matter **17**, R705 (2005).
[13]A. Karimi, S. Yazdi, and A. M. Ardekani, Biomicrofluidics **7**, 021501 (2013).
[14]M. He, C. Sun, and D. T. Chiu, Anal. Chem. **76**, 1222 (2004).
[15]M. Abdelgawad, S. L. S. Freire, H. Yang, and A. R. Wheeler, Lab Chip **8**, 672 (2008).
[16]H. Yang, J. M. Mudrik, M. J. Jebrail, and A. R. Wheeler, Anal. Chem. **83**, 3824 (2011).
[17]X. C. i Solvas, V. Turek, T. Prodromakis, and J. B. Edel, Lab Chip **12**, 4049 (2012).
[18]G. Serge and A. Silberberg, Nature **189**, 209 (1962).
[19]P. G. Saffman, J. Fluid Mech. **22**, 385 (1965).
[20]E. S. Asmolov, Fluid Dyn. **25**, 886 (1990).
[21]N. Raju and E. Meiburg, Phys. Fluids **9**, 299 (1997).
[22]J. P. Matas, J. F. Morris, and E. Guazzelli, Oil Gas Sci. Technol. **59**, 59 (2004).
[23]D. D. Carlo, D. Irimia, R. G. Tompkins, and M. Toner, Proc. Natl. Acad. Sci. U.S.A. **104**, 18892 (2007).

[24]P. Paik, V. K. Pamula, M. G. Pollack, and R. B. Fair, Lab Chip **3**, 28 (2003).
[25]S. K. Cho, H. Moon, and C.-J. Kim, J. Microelectromech. Syst. **12**, 70 (2003).
[26]F. Mugele, J.-C. Baret, and D. Steinhauser, Appl. Phys. Lett. **88**, 204106 (2006).
[27]S. H. Ko, H. Lee, and K. H. Kang, Langmuir **24**, 1094 (2008).
[28]H. Lee, S. Yun, S. H. Ko, and K. H. Kang, Biomicrofluidics **3**, 044113 (2009).
[29]F. Mugele, A. Staicu, R. Bakker, and D. van den Ende, Lab Chip **11**, 2011 (2011).
[30]C.-P. Lee, H.-C. Chen, and M.-F. Lai, Biomicrofluidics **6**, 012814 (2012).
[31]P. García-Sánchez, A. Ramos, and F. Mugele, Phys. Rev. E **81**, 015303R (2010).
[32]J. M. Oh, D. Legendre, and F. Mugele, EPL **98**, 34003 (2012).
[33]H. B. Eral, D. Mampallil, M. H. G. Duits, and F. Mugele, Soft Matter **7**, 4954 (2011).
[34]D. Mampallil, H. B. Eral, D. van den Ende, and F. Mugele, Soft Matter **8**, 10614 (2012).
[35]D. Mampallil, D. van den Ende, and F. Mugele, Appl. Phys. Lett. **99**, 154102 (2011).
[36]F. Sbalzarini and P. Koumoutsakos, J. Struct. Biol. **151**, 182 (2005).
[37]J. P. Shelby, D. S. W. Lim, J. S. Kuo, and D. T. Chiu, Nature **425**, 38 (2003).
[38]T. Karino and H. L. Goldsmith, Microvasc. Res. **17**, 217 (1979).
[39]A. J. Mach, J. H. Kim, A. Arshi, S. C. Hur, and D. D. Carlo, Lab Chip **11**, 2827 (2011).
[40]B. R. Lutz, J. Chen, and D. T. Schwartz, Anal. Chem. **78**, 5429 (2006).
[41]K. Chong, S. D. Kelly, S. Smith, and J. D. Eldredge, Phys. Fluids **25**, 033602 (2013).
[42]C. Karuwan, K. Sukthang, A. Wisitsoraat, D. Phokharatkul, V. Patthanasettakul, W. Wechsatol, and A. Tuantranont, Talanta **84**, 1384 (2011).